Materials Science Forum Vols. 384-385 (2002) pp. 241-248
© 2002 Trans Tech Publications, Switzerland

Ultrafast & Highly Efficient Resonant Cavity Enhanced Photodiodes

E. Ozbay[1], I. Kimukin[1], and N. Biyikli[2]

[1] Department of Physics, Bilkent University, 06533 Ankara, Turkey

[2] Department of Electrical and Electronics Engineering, Bilkent University, 06533 Ankara, Turkey

biyikli@fen.bilkent.edu.tr

Keywords: High-speed Photodetectors, Resonant Cavity Enhancement, Schottky Diode, p-i-n Photodiode, Quantum Efficiency.

Abstract. In this paper, we review our research efforts on resonant cavity enhanced (RCE) high-speed high-efficiency p-i-n and Schottky photodiodes (PDs) operating in the 1st optical communication window. Using a microwave compatible planar fabrication process, we have designed and fabricated GaAs based RCE photodiodes. For RCE Schottky type photodiodes, we have achieved peak quantum efficiencies of 50% and 75% with semi-transparent (Au) and transparent (indium-tin-oxide) Schottky layers, respectively. Along with 3-dB bandwidths of 50 and 60 GHz, these devices exhibit bandwidth-efficiency (BWE) products of 25 GHz and 45 GHz respectively. For RCE p-i-n type photodiodes, we have fabricated and tested widely tunable devices with 92% quantum efficiency, along with a 3-dB bandwidth of 50 GHz, resulting in a 46 GHz BWE performance. These results correspond to the highest detector performances reported for vertically illuminated Schottky and p-i-n PDs in scientific literature.

Introduction

As the information revolution continues at an increasing pace, there is an exponentially increasing demand for larger telecommunication bandwidths. The optical communication systems are currently the only viable solution for this bandwidth demand. Optoelectronic components such as semiconductor lasers, photodetectors, modulators, and optical amplifiers are at the heart of these communication systems, and the performance of all these devices should be increased to meet the existing and expected bandwidth requirements. Besides the optical communication systems, high-performance photodetectors are also vital components of optical measurement systems [1,2]. Both Schottky PDs [3-5] and p-i-n PDs [6,7] offer high-speed performance to fulfill the needs of such systems. However, the efficiency of these detectors has been typically limited to less than 10%, mostly due to the thin absorption region needed for short transit times. One can increase the absorption region thickness to achieve higher efficiencies, but this also means longer transit times that will degrade the high-speed performance of the devices. RCE photodetectors offer the possibility of overcoming this limitation in the BWE product of conventional PDs [8-10]. High-speed RCE photodetector research has mainly concentrated on using p-i-n PDs [11] and avalanche PDs, where 35 GHz low-gain bandwidth [12] and 17 GHz BWE performance [13] have been reported. In our work, with p-i-n type RCE PDs we achieved >90% quantum efficiency along with a 50 GHz performance [14]. We have fabricated RCE Au-Schottky PDs with 50% quantum efficiency and a 50 GHz frequency performance [15]. Recently, we have improved the performance of RCE Schottky type PDs to 60 GHz bandwidth, along with a 75% quantum efficiency via a transparent Schottky layer and top dielectric Bragg mirror [16]. In this paper, we review our recent work on design, fabrication and characterization of high performance RCE PDs.

Theory of Resonant Cavity Enhancement in Photodetectors

The well-known BWE trade-off is a major blockade for using high-speed PDs in long-haul telecommunications. As the active region thickness is decreased to minimize the transit time for high-speed purposes, the quantum efficiency of the same device proportionally decreases. For a PD with transit-time limited frequency response, the 3-dB bandwidth can be formulated as

$$f_{3dB} \approx 0.45\frac{v}{d}, \quad (1)$$

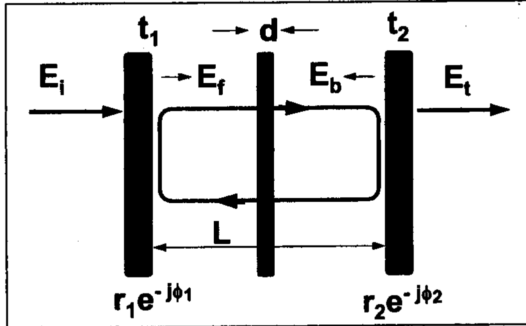

Figure 1. Schematics of the Fabry Perot cavity model. The shaded absorption region was used to simulate the active region placed in the cavity.

where ν is the drift velocity of the charge carrier, and d is the active region thickness. For thin active regions, the absorption can be formulated as

$$\eta = (1-R)(1-e^{-\alpha d}) \approx (1-R)\alpha d\,, \tag{2}$$

where α is the power absorption loss factor of the optical field within the active region, and αd <<1 is assumed. Using equations (1) and (2), the BWE product can be obtained as,

$$f_{3dB} \cdot \eta = 0.45(1-R)v\alpha\,, \tag{3}$$

which is independent of the active region thickness.

This BWE trade-off can be solved by placing the active region in a Fabry-Perot cavity (Fig.1). This is usually achieved by integrating the photoactive region with a bottom Bragg mirror. In a Fabry-Perot cavity, the optical field is enhanced resulting in increased efficiencies. The electric field component for the forward traveling wave E_f inside the cavity (Fig. 1) can be related to the incident field E_i as:

$$E_f = \frac{t_1}{1-r_1 r_2 e^{-\alpha d} e^{-j(2\beta L+\phi_1+\phi_2)}} E_i\,, \tag{4}$$

where $r_1 e^{j\phi 1}$ and $r_2 e^{j\phi 2}$ are the reflection coefficients of the mirrors, t_1 is the transmission coefficient of the front mirror, β is the propagation constant for the traveling EM wave in air, and L is the total width of the cavity. The backward traveling wave E_b is related to E_f as:

$$E_b = r_2 e^{-\alpha d} e^{-j(\beta L+\phi_2)} E_f\,. \tag{5}$$

Using equations (4) and (5), we can calculate the power enhancement factor η, which is defined as the ratio of the absorbed power inside the absorption layer, to the power of the incident EM wave,

$$\eta = \frac{(1+R_2 e^{-\alpha d})(1-R_1)}{1-2\sqrt{R_1 R_2}e^{-\alpha d}\cos(2\beta d+\phi_1+\phi_2)+R_1 R_2 e^{-\alpha d}} \tag{6}$$

where $R_1 = r_1^2$ and $R_2 = r_2^2$, are the reflectivities of the mirrors of the cavity. The above result is normalized with respect to the incident field absorbed by the detector in the absence of the cavity. As can be seen from equation (6), the introduction of a Fabry-Perot cavity can increase the quantum efficiency without effecting the high-speed properties. Besides, the detector becomes wavelength selective which may be very useful for wavelength division multiplexing (WDM) based optical communication systems.

Resonant Cavity Enhanced PIN Photodiodes

As mentioned earlier, p-i-n photodiodes are also widely used in telecommunication systems. The details of the p-i-n photodiode epitaxial structure we have used in this work is given in Table 1. In this structure, the bottom Bragg mirror is made of quarter-wave stacks ($Al_{0.20}Ga_{0.80}As/AlAs$) designed for high reflectance at 820 nm center wavelength. Carrier trapping was avoided by using linear composition grading at interfaces of the absorbing layer. The active layer thickness, d, was chosen such that the maximum quantum efficiency is obtained by,

$$R_1 = R_2 e^{-2\alpha d} \tag{7}$$

where α is the absorption coefficient, R_1 is the top air-semiconductor mirror reflectance, and R_2 is the bottom Bragg mirror reflectance [8]. The reflectivity measurements are used to investigate the epitaxial structure of the wafer. The resonance occurs at 826 nm with a measured reflectance minimum of 5%, while our theoretical simulations predict nearly zero reflectance at the same wavelength. The measured resonance wavelength changes from 826 nm at the center of the wafer, to 816 nm at the edge of the wafer. This epilayer thickness variation across the wafer and small deviations between growth and design explain the difference between the theoretical and experimental reflectance characteristics.

The samples were fabricated by a microwave-compatible fabrication process. First, ohmic contacts to the N+ layers were formed by a recess etch that was followed by a self-aligned Au-Ge-Ni liftoff. The p+ ohmic contact was achieved by an Au/Ti lift-off. The samples were then rapid thermal annealed. Using an isolation mask, we etched away all of the epilayers except the active areas. Then, we evaporated Ti/Au interconnect metal which formed coplanar waveguide (CPW) transmission lines on top of the semi-insulating substrate. The next step was the deposition and patterning of a 2000 Å thick silicon nitride layer. Finally, a 1.0 micron thick Au layer was used as an airbridge to connect the center of the CPW to the top p+ ohmic metal. The resulting p-i-n diodes had breakdown voltages larger than 15 V.

Photoresponse measurements were carried out in the 750-850 nm wavelength range by using a tungsten-halogen projection lamp as the light source and a single pass monochromator. The output of the monochromator was coupled to a multimode fiber. The monochromatic light was delivered to the devices by a lightwave fiber probe, and the electrical characterization was carried out on a probe station. The spectral response was measured using a calibrated optical powermeter. For photospectral measurement, large area photodiodes (250 μm x 250 μm) were chosen to ensure all of the optical power is incident on the active area. The top p^+ layers were recess etched in small steps, and the tuning of the resonance wavelength within the Bragg mirror's upper and lower edges was observed.

Material	Doping (cm^{-3})	Thickness (nm)
GaAs	p^+ $2x10^{18}$	20
$Al_{0.2}Ga_{0.8}As$	p^+ $2x10^{18}$	200
$Al_{0.2}Ga_{0.8}As$ → GaAs	undoped	38
GaAs	undoped	470
GaAs → $Al_{0.2}Ga_{0.8}As$	undoped	38
$Al_{0.2}Ga_{0.8}As$	n^+ $2x10^{18}$	390
$Al_{0.2}Ga_{0.8}As$	undoped	180
$Al_{0.20}Ga_{0.80}As/AlAs$ Bragg Mirror	undoped	24 x (59 / 68)
Semi-Insulating GaAs Substrate		

Table 1: Epitaxial structure of RCE PIN Photodiode

Fig. 2 shows the spectral quantum efficiencies of devices with different recess etch. Device 1 corresponds to as-grown wafer, while devices 2, 3, and 4 have been recess etched 21, 44, and 79 nm respectively. The no-etch peak quantum efficiency (86%) increases to 92% after the top absorbing GaAs cap layer is removed.

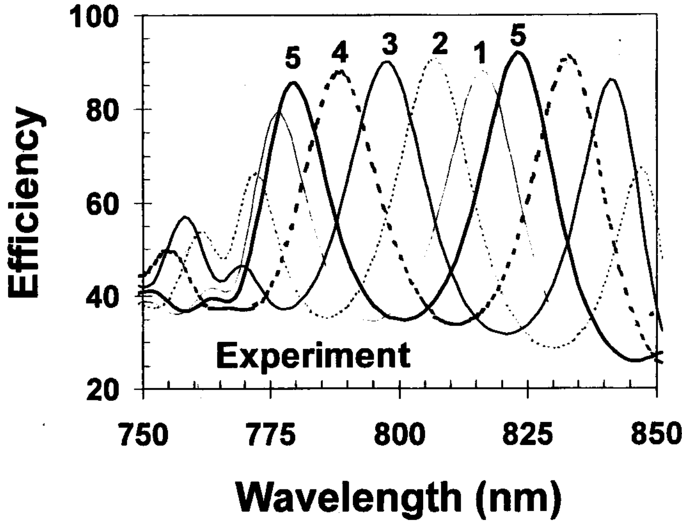

Figure 2: (a) Experimental photoresponse of the RCE p-i-n photodiode.

The peak quantum efficiency remains almost constant afterwards until the resonance wavelength reaches to the lower edge of the Bragg mirror (790 nm). At this point, the second resonance appears around the upper edge of the Bragg mirror. As seen in Fig. 2, the resonance wavelength can be tuned from 780 nm to 845 nm with peak efficiencies above 85%. The full-width at half maximum (FWHM) of the devices is around 15 nm. The data shown in Fig. 2 is obtained at zero bias. The measured quantum efficiencies do not change at higher reverse biases, as the undoped active region is already depleted at zero bias.

High speed measurements were made with 1 ps FWHM optical pulses obtained from a Ti-Sapphire laser operating at 820 nm. Figure 3 shows the temporal response of a small area photodiode measured by a 50 GHz sampling scope. The measured photodiode output has a 12 ps FWHM. The Fourier transform of the data has a 3-dB bandwidth of 38 GHz. The measured data are corrected by deconvolving the scope response, which is assumed to be a Gaussian pulse with a 7 ps rise time. After this correction, the device has a 3 dB bandwidth of 50 GHz, which corresponds to the highest frequency response reported for p-i-n type RCE photodiodes.

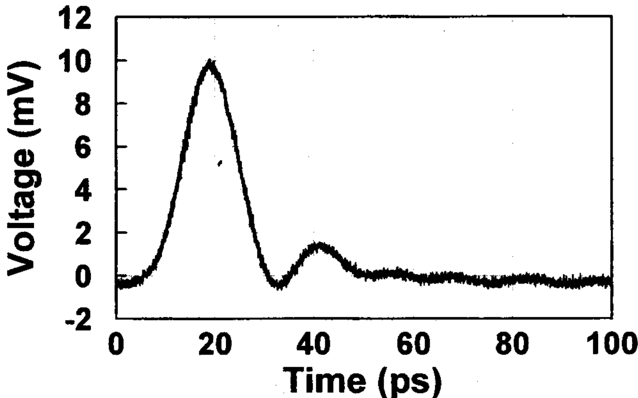

Figure 3: Pulse response of the sample

We calculated the theoretical frequency response of the device as described in Ref. 15. The device under test has an RC time constant of 1.2 ps, corresponding to a 3 dB bandwidth of 230 GHz. The response of the device is mostly limited by the hole (7.5 ps) and electron (4.5 ps) transit times. Using these numerical values, we predict a 3 dB bandwidth of 50 GHz for the device under test, in good agreement with the deconvolved high-speed measurements. In terms of detector performance, which is determined by the BWE product, our RCE p-i-n PDs have a BWE product of 92% x 50 GHz = 46 GHz. Our analysis reveals that the 3 dB bandwidth of the p-i-n structure can be further increased to >100 GHz by using a thinner active region. For that case a dielectric top Bragg mirror can be used to achieve >90% quantum efficiencies, which will yield a device with a bandwidth-efficiency product in excess of 100 GHz.

Resonant Cavity Enhanced Schottky Photodiodes

We've designed, fabricated and characterized RCE Schottky PDs with semi-transparent (thin Au metal) and transparent (indium-tin-oxide (ITO)) Schottky layers. The BWE performance obtained from these devices are 25 GHz and 45 GHz respectively. Both diode structures were similarly designed using transfer-matrix-method (TMM) based theoretical simulations, except that the RCE Au-Schottky PD design had 18 pair bottom Bragg mirror whereas the RCE ITO-Schottky PD design had a bottom Bragg mirror of 24 pairs of $Al_{0.20}Ga_{0.80}As/AlAs$ alternating $\lambda/4$-thick layers. A ~150 nm thick GaAs active layer was used in both designs, which was the only absorbing part of the detector cavity at the design wavelength of 820 nm. All the cavity layers except the GaAs photo-absorption layer were designed as $Al_{0.20}Ga_{0.80}As$ which is transparent at the operation wavelength. Therefore, no diffusion component of the photocurrent was expected in these heterostructure RCE-PD designs which improves high-frequency performance of these devices. The samples were fabricated by a microwave-compatible process similar to the one used for the pin photodiodes.

RCE Au-Schottky PDs: A thin (~10 nm) semitransparent Au film is deposited via thermal evaporation as the Schottky contact in these devices. As Schottky contact material, Au has excellent electrical properties and forms high-quality Schottky barriers with GaAs. The Au film also functions as the top mirror of the resonant cavity. However, it absorbs a significant portion of the incident light, thereby decreasing the efficiency of the detector. Moreover, the thin Au film has large surface fluctuations which causes scattering of incident optical field. Fig. 4 shows the photoresponse of the fabricated RCE Au-Schottky PDs. The peak quantum efficiency is 50% around 827 nm under 2.5 V reverse bias. This value corresponds to a five-fold enhancement of the efficiency of a single-pass conventional PD with the same active layer thickness.

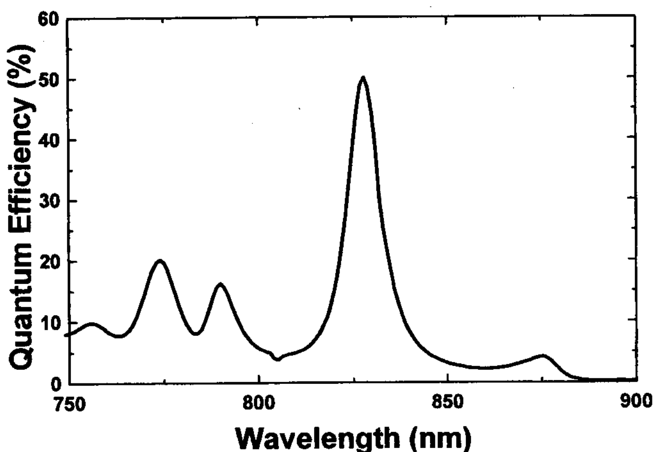

Figure 4: Spectral photoresponse of RCE Au-Schottky photodiode.

High-speed measurements were done using the similar high-frequency set-up described in the previous section. The best measured FWHM is 12 psec under 8 V reverse bias. Considering a 9 psec FWHM for the 50 GHz scope, the deconvolved pulse response has a 3-dB bandwidth of ~50 GHz. The detector response becomes considerably slower for reverse biases lower than 6 V. This observation indicates that a 6 V reverse bias is needed for full depletion of the absorbing GaAs layer, which is a result of the relatively high-doping in the depletion region.

RCE ITO-Schottky PDs: ITO, which is known to be a transparent conductor, is a potential alternative to thin semi-transparent Au as the Schottky-contact material. Its transparency minimizes the problem of optical loss and scattering, resulting in higher efficiency performance [17,18]. However, due to its low refractive index ITO films show poor reflectivity. Therefore, for optimum RCE effect we need an additional top mirror.

The deposition of the Schottky-contact material ITO was done via RF magnetron sputtering in an Ar environment from a composite target containing by weight 90% In_2O_3 and 10% SnO_2. Before device fabrication, electrical and optical properties of sputtered thin ITO films were characterized. The resistivity of the as-grown ITO film was determined approximately as $2x10^{-4}$ Ω-cm. This value decreased to $1.5x10^{-4}$ Ω-cm and $1.2x10^{-4}$ Ω-cm when the films were annealed at 300 °C and 400 °C, respectively. Using a fiber-optic based optical transmission measurement set-up, the transmittivity of a 150 nm-thick ITO film deposited on a quartz substrate was measured. The transmittivity was around 87% at 820 nm, and increased very slightly (to ~88%) with annealing up to 450 °C. Reflectivity at the same wavelength was measured to be 12% before annealing, which indicated that the absorption in ITO film was ~1%. Another important optical property was the refractive index of the film, which was measured by an ellipsometer. The measured refractive index of the as-grown ITO film was 1.99, and this value decreased to 1.85 after the film was annealed at 450 °C. These results showed that the sputtered ITO films could be used as low-loss, high-quality Schottky contacts to our devices.

After the device fabrication is completed, the top mirror of the resonant cavity was formed by a PECVD-grown dielectric Si_3N_4/SiO_2 DBR centered at 820 nm. The resulting RCE-Schottky PDs had breakdown voltages around 8 V and typical dark current densities were $5x10^{-5}$ A/cm^2 at -1 V bias. By current-voltage measurements, the Schottky barrier height and the ideality factor of the ITO/GaAs Schottky contacts were determined as 0.74 eV and 1.12 respectively. Fig. 5 shows the picture of a fabricated small area high-speed RCE ITO-Schottky PD.

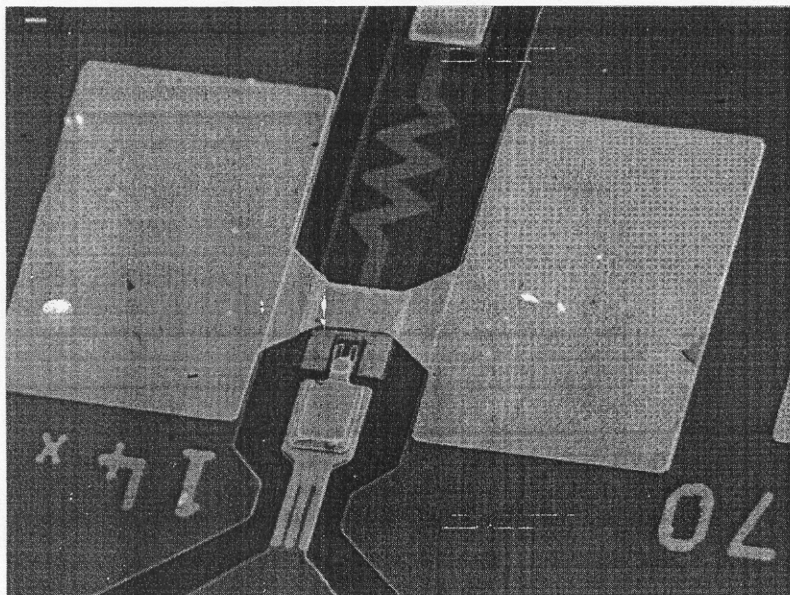

Figure 5: Scanning electron microscope picture of a fabricated high-speed RCE ITO-Schottky photodiode.

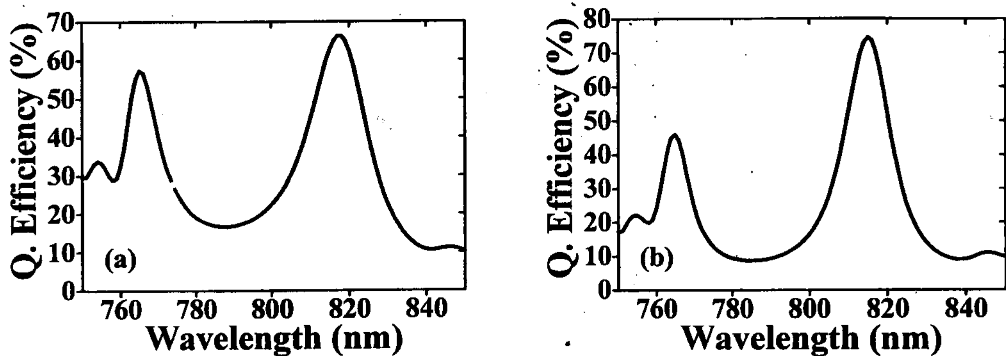

Figure 6: Spectral quantum efficiency of the RCE ITO-Schottky PD (a) without top DBR (b) with 2-pair top DBR

Fig. 6(a) shows the spectral quantum efficiency measurement of the RCE-Schottky PD without a dielectric top DBR mirror. The spectral quantum efficiency of the same device with a 2 pair Si_3N_4/SiO_2 top Bragg mirror is shown in Fig. 6(b). The peak quantum efficiency before top DBR deposition was 66% at 817 nm and increased to a maximum of 75% at 815 nm for a 2 pair top DBR mirror. Both measurements were done at zero bias. The peak quantum efficiency did not change with applied bias voltage, which indicated that the diode active layer was completely depleted.

High-speed measurements were implemented by utilizing a picosecond mode-locked Ti:sapphire laser, which was tuned at the resonant wavelength of our detectors, 815 nm. The devices were illuminated by a single-mode fiber on a microwave probe station and the resulting pulses were observed on a 50-GHz sampling scope. The pulse response of the detector was observed to be bias dependent. While 12 psec FWHM was measured at zero bias, this value decreased to 11.5 psec for 2 V reverse bias voltage. The best measured data had a FWHM of 11.2 psec under a reverse bias of 4 V. Further increase of the bias voltage made the PD response slower, mainly due to the avalanche gain mechanism, which was significant for bias voltages higher than 5 V. Fig. 7 shows the measured temporal response of a small area (5x5 μm^2) RCE ITO-Schottky PD under 4 V reverse bias. The Fourier transform of the temporal data has a 3-dB bandwidth of 43 GHz. The measured data was corrected by deconvolving the scope response. Considering a 9 psec FWHM for the 50 GHz scope, our detectors had a 3-dB bandwidth of 60 GHz. The inset figure in Fig. 7 shows the as-measured and deconvolved frequency responses obtained from the fast Fourier transform (FFT) of the temporal detector response. The efficiency and bandwidth measurements of the fabricated RCE ITO-Schottky PDs resulted in a detector performance of 45 GHz BWE product.

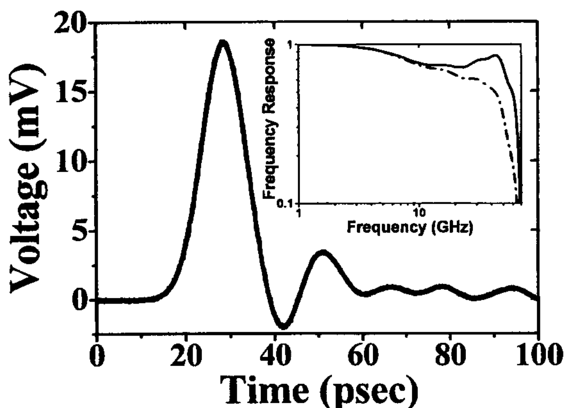

Figure 7. Pulse response of a 5x5μm^2 RCE ITO-Schottky PD. The inset shows the as-measured (dashed line) and deconvolved (solid line) frequency responses of the detectors.

Conclusion

In summary, we reviewed our recent work on ultrafast high-efficiency resonant cavity enhanced photodetectors. Using a microwave compatible planar fabrication process, we have designed and fabricated GaAs based RCE PDs. For RCE p-i-n type PDs, we have achieved a BWE performance of 46 GHz. For RCE Schottky type photodiodes, we have improved the 25 GHz BWE performance to 45 GHz BWE by using a transparent ITO-Schottky layer and a dielectric top Bragg mirror instead of semitransparent Au-Schottky metal. To the best of our knowledge, these BWE values correspond to the highest detector performances reported for vertically illuminated p-i-n and Schottky photodiodes.

Acknowledgements

This work was supported by NATO Grant No. SfP971970, National Science Foundation Grant No. INT-9906220, Turkish Department of Defense Grant No. KOBRA-001 and Thales JP8.04

References

[1] J. E. Bowers and Y. G. Wey in *Handbook of Optics*, chap. 17, McGraw-Hill, New York, (1995).

[2] K. Kato, IEEE Trans. Microwave Theory Tech. **47**, pp. 1265-1281, 1998.

[3] S. Y. Wang, and D. M. Bloom, Electron. Lett. **19**, pp. 554-555, 1983.

[4] E. Özbay, K. D. Li, and D. M. Bloom, IEEE Photon. Technol. Lett. **3**, pp. 570-572, 1991.

[5] K. D. Li, A. S. Hou, E. Özbay, and D. M. Bloom, Appl. Phys. Lett. **61**, pp. 3104-3106, 1992.

[6] Y. G. Wey, M. Kamegawa, A. Mar, K. J. Williams, K. Giboney, D. L. Crawford, J. E. Bowers, and M. J. Rodwell, J. Lightwave Technol.**13**, pp. 1490-1494, 1995.

[7] Y. G. Wey, K. S. Giboney, J.E. Bowers, M. J. W. Rodwell, P. Silvestre, P. Thiagarajan, and G.Y. Robinson, IEEE Photon. Technol. Lett. **5**, pp. 1310-1312, 1993.

[8] M. S. Ünlü and S. Strite, J. Appl. Phys. Rev. **78**, pp. 607-628, 1995.

[9] K. Kishino, M. S. Ünlü, J. I. Chyi, J. Reed, L. Arsenault, and H. Morkoç, IEEE J. Quantum Electron. **27**, pp. 2025-2031, 1991.

[10] I. H. Tan, E. L. Hu, and J. E. Bowers, IEEE J. Quantum Electron. **31**, pp. 1863-1869, 1995.

[11] C. C. Barron, C. J. Mahon, B. J. Thibeault, G. Wang, W. Jiang, L. A. Coldren, and J. E. Bowers, Electron. Lett. **30**, pp. 1796-1797, 1994.

[12] P. Yuan, O. Baklenov, H. Nie, A. L. Holmes, B. G. Streetman, and J. C. Campbell, IEEE J. Select. Topics in Quantum Electron.. **6**, pp. 422-424, 2000.

[13] C. Lennox, H. Nie, P. Yuan, G. Kinsey, A. L. Holmes, B. G. Streetman, and J. C. Campbell, IEEE Photon. Technol. Lett. **11**, pp. 1162-1164, 1999.

[14] E. Ozbay, I. Kimukin, N. Biyikli, O. Aytur, M. Gokkavas, G. Ulu, M. S. Unlu, R. P. Mirin, K. A. Bertness, and D. H. Christensen, Appl. Phys. Lett. **74**, pp. 1072-1074, 1999.

[15] M. S. Unlu, M. Gokkavas, B. M. Onat, E. Ata, E. Ozbay, R. P. Mirin, K. J. Knopp, K. A. Bertness, and D. H. Christensen, Appl. Phys. Lett. **72**, pp. 2727-2729, 1998.

[16] N. Biyikli, I. Kimukin, O. Aytür, M. Gökkavas, M. S. Ünlü, and E. Ozbay, to appear in July, 2001 issue of IEEE Photonics Technology Letters.

[17] D. G. Parker, P. G. Say, and A. M. Hansom, Electron. Lett. **23**, pp. 527-528, 1987.

[18] W. A. Wohlmuth, J.-W. Seo, P. Fay, C. Caneau, and I. Adesida, IEEE Photon. Technol. Lett. **9**, pp. 1388-1390, 1997.